INTERNATIONAL JOURNAL FOR NUMERICAL METHODS IN FLUIDS, VOL. 3, 1–21 (1983)

A TRANSONIC QUASI-3D ANALYSIS FOR GAS TURBINE ENGINES INCLUDING SPLIT-FLOW CAPABILITY FOR TURBOFANS

W. G. HABASHI*

Concordia University, Montreal, Quebec, Canada

G. G. YOUNGSON†

Pratt & Whitney Aircraft of Canada, Longueuil, Quebec, Canada

SUMMARY

A numerical approximation is taken to the solution of the complex flows existing in gas turbine engines with transonic blading. The quasi-3D approach decouples the problem into through-flow and blade-to-blade solutions. An industrially practical finite element through-flow solution is developed and for blade-to-blade solutions a transonic finite areas method is utilized. The finite element code developed is capable of operating in an analysis or a design mode. In both modes a dynamic relaxation factor is employed and considerable reduction in solution time can be achieved. Comparisons to streamline curvature methods are carried out for simple analytical and complex industrial problems.

KEY WORDS Turbomachines Finite Elements Transonic Flows

1. INTRODUCTION

The aerodynamic flows within turbomachines are of sufficient complexity to warrant considerable simplifying assumptions before a numerical solution is attempted. The actual flow is unsteady, three-dimensional, compressible and viscous. The solution of the Navier–Stokes equations is a formidable task. Even with the advent of three-dimensional solutions, aerodynamic designers are best served, at least in the preliminary stages, by two-dimensional sectional information.

Numerical analysis of the flows in turbomachines has in general followed the Wu[1] theory. In this theory, three-dimensional flows are decoupled and calculated on two families of intersecting stream surfaces. Flows are calculated independently on the S1 (blade-to-blade) surfaces and on the S2 (hub-to-shroud) surface. Linkage terms exist between the two families. An iterative procedure is required to generate a quasi-3D solution, with the solution on one surface feeding into the other until global convergence is achieved.

The three main approaches to the through-flow problem are (1) Streamline curvature methods (SCM), (2) Matrix or finite difference methods (FDM), (3) Finite element methods (FEM).

Extensive calculations have been made using the first two methods[2–7] and comparisons between them have been carried out by several authors.[8,9] The finite element method is a

---

* Associate Professor; also Consultant, Pratt & Whitney Aircraft of Canada.
† Aerodynamicist.

0271–2091/83/010001–21$02.10 *Received 6 August 1981*

recent newcomer to this field,[10–12] but is quickly establishing itself as particularly well-suited to tackling the through-flow problem. Habashi[13] gives a summary and review of the three methods.

All three methods start from the assumptions of steady, inviscid flow and numerically solve the radial component of the Navier–Stokes equation to establish a velocity-density field satisfying the continuity equation. Passage-averaged continuity, momentum, and energy equations are derived and are assumed to hold in a plane $\theta = \text{constant}$. Alternatively the solution can be viewed as that on a mean blade-to-blade stream surface whose shape is given by the geometry of the blade rows. Methods, however, differ in their choice of the mean S2 surface or streamsheet.

Once the streamsheet shape has been selected the flow field is broken down into a network which depends on the solution method and the unknowns are determined at each of these nodal points. With the blade geometry given, a cascade model is used to determine the air deflection and the pressure loss. Boundary layer growth along the hub and shroud can be calculated and specified as a blockage factor whose effect could be included by recalculating new hub and shroud displaced geometries.

In the present work we address ourselves to both the through-flow analysis and design problems as perceived in an industrial situation. We also combine the developed through-flow analysis with the finite areas method (FAM) of McDonald[14] to form an automated quasi-3D solver. It should be mentioned that finite element methods for transonic blade-to-blade solutions, based on artificial compressibility, have developed rapidly in the last few years[15–17] and now handle transonic or supersonic cascade flows with shocks. With such schemes it will be possible to handle the entire transonic quasi-3D approach using a finite element method.

2. GOVERNING EQUATIONS AND BOUNDARY CONDITIONS

Governing equations

The radial equilibrium equation can be written as:

$$C_x\left[\frac{\partial C_r}{\partial x}-\frac{\partial C_x}{\partial r}\right]-\frac{V_u}{r}\frac{\partial(rC_u)}{\partial r}=T\frac{\partial s}{\partial r}-\frac{\partial I}{\partial r} \tag{1}$$

where:

x = axial co-ordinate
r = radial co-ordinate
u = circumferential co-ordinate
V = relative velocity
C = absolute velocity
T = temperature
I = rothalpy
s = entropy

By defining:

$$C_x=\frac{\dot{m}}{2\pi\rho rb}\frac{\partial\Psi}{\partial r} \tag{2}$$

$$C_r=\frac{-\dot{m}}{2\pi\rho rb}\frac{\partial\Psi}{\partial x} \tag{3}$$

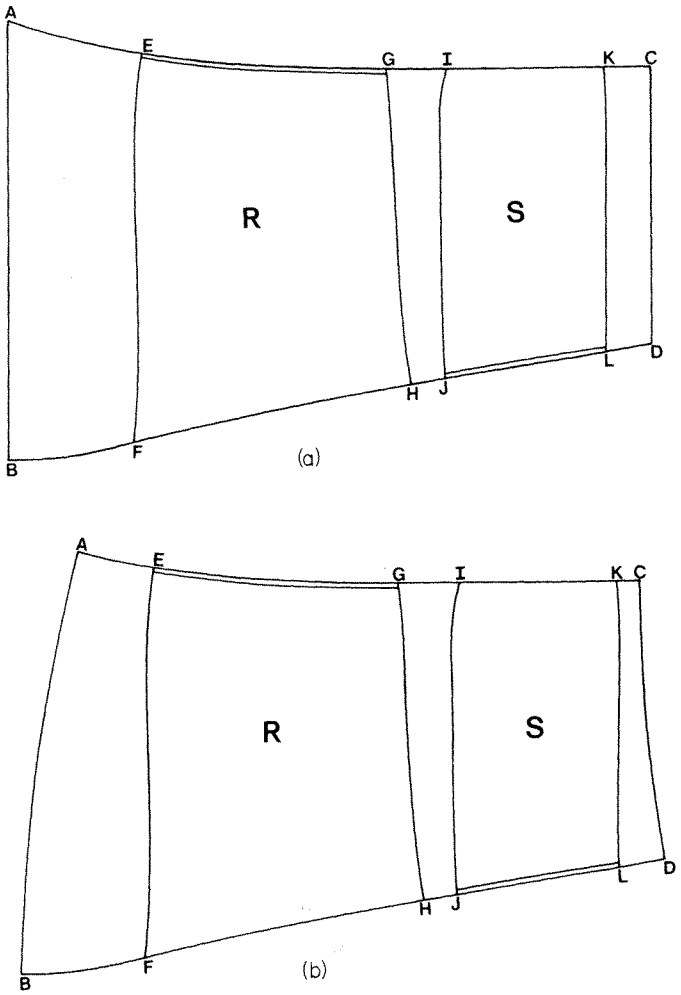

Figure 1. Flow geometry and boundary conditions

equation (1) can be rewritten as:

$$\frac{\partial}{\partial r}\left(\frac{1}{\rho r b}\frac{\partial \Psi}{\partial r}\right)+\frac{\partial}{\partial x}\left(\frac{1}{\rho r b}\frac{\partial \Psi}{\partial x}\right)=\frac{-1}{C_x}\left[\frac{V_u}{r}\frac{\partial (rC_u)}{\partial r}+T\frac{\partial s}{\partial r}-\frac{\partial I}{\partial r}\right]\frac{2\pi}{\dot{m}}=G \tag{4}$$

where b = blockage factor and the boundary conditions of Figure 1b are:

on hub, BD : $\Psi = 0$

on shroud, AC : $\Psi = 1$

at inlet, AB : $\dfrac{\partial \Psi}{\partial n} = 0$ (5)

at exit, CD : $\dfrac{\partial \Psi}{\partial n} = 0$, where n is the outward normal.

A quasi-variational integral corresponding to (4) is:

$$J(\Psi)=\frac{1}{2}\iint\frac{1}{\rho rb}\left[\left(\frac{\partial\Psi}{\partial x}\right)^2+\left(\frac{\partial\Psi}{\partial r}\right)^2\right]+2\Psi G\Big]\,dr\,dx-\oint\frac{\Psi}{\rho rb}\frac{\partial\Psi}{\partial n}\,ds \tag{6}$$

which upon minimization yields:

$$[K]\{\Psi\}=\{F\} \tag{7}$$

where

$$k_{ij}=\iint\frac{1}{\rho rb}\left[\left(\frac{\partial\Psi}{\partial r}\right)^2+\left(\frac{\partial\Psi}{\partial x}\right)^2\right]dr\,dx \tag{8}$$

$$F_i=\iint\frac{1}{C_x}\left[\frac{V_u}{r}\frac{\partial(rC_u)}{\partial r}+T\frac{\partial s}{\partial r}-\frac{\partial I}{\partial r}\right]\frac{2\pi}{\dot{m}}\,dr\,dx \tag{9}$$

In most previous works the contour integral of equation (6) is assumed to vanish since on all boundaries Ψ is either a constant (hub or shroud) or $\partial\Psi/\partial n=0$ (parallel inlet and exit), (Figure 1(a)). In many engines, for example the Pratt and Whitney of Canada PT6, inlets are

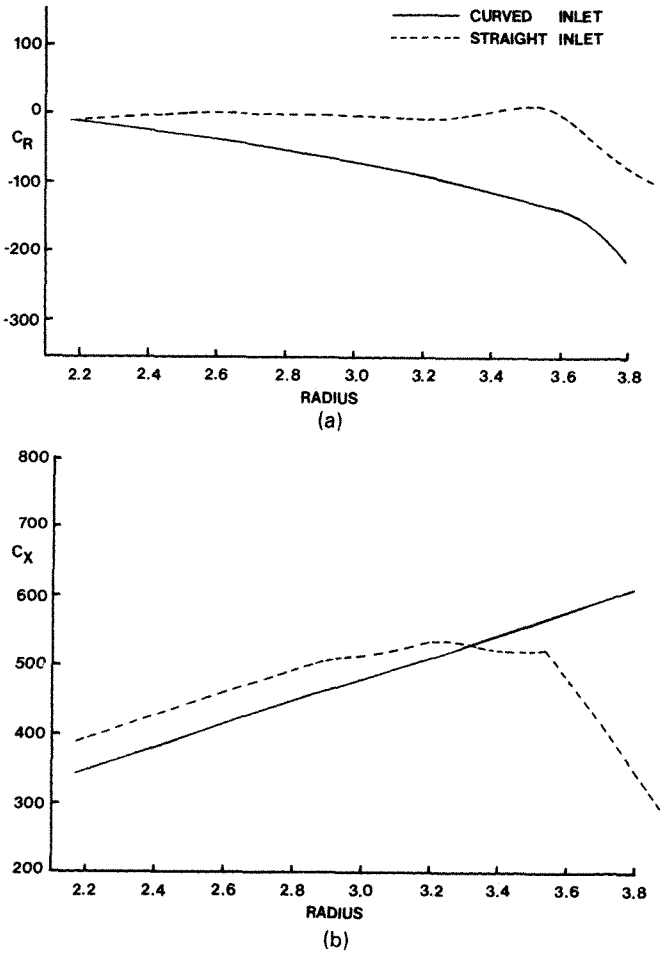

Figure 2. Comparison between straight and curved inlets

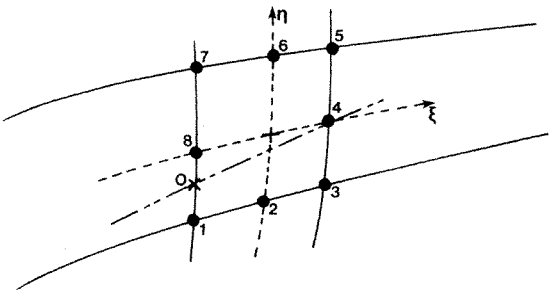

Figure 3. Isoparametric formulation of 8-node quadrilaterals

far from uniform. Solutions are obviously quite sensitive to the imposed boundary conditions at the inlet and the exit. In the present work we maintain $\partial\Psi/\partial n = 0$ by building an inlet and exit that are, as much as possible, normal to the streamlines at these stations (Figure 1(b)). The effect of building such an inlet is dramatic, as shown in Figure 2 for the inlets and exits shown in Figure 1. We note in Figure 2(a) the non-physical distribution of radial velocity at the inlet resulting from the use of a radial first station. By adopting the inlet of Figure 1(b), both distributions of C_x and C_r become more realistic.

3. FINITE ELEMENT DISCRETIZATION

We adopt the curvilinear eight-node isoparametric element where both function, Ψ, and geometry have parabolic representation. In each element

$$\Psi = \sum_{i=1}^{8} N_i(\xi, \eta)\Psi_i \tag{10}$$

$$x = \sum_{i=1}^{8} N_i(\xi, \eta)x_i \tag{11}$$

$$r = \sum_{i=1}^{8} N_i(\xi, \eta)r_i \tag{12}$$

N_i being the shape functions of the finite element written in terms of the local co-ordinates ξ and η, shown in Figure 3. The mid-nodes of the curvilinear elements are obtained by the exact procedure shown in Figure 4.

In an industrial atmosphere where a through-flow program may be heavily utilized in a design or an analysis mode it becomes imperative to devise a reliable and efficient automated finite element mesh generation procedure. Our present program is totally automated and

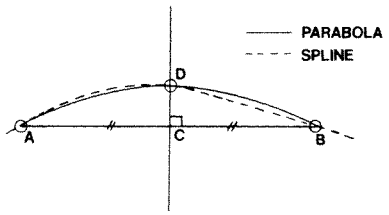

Figure 4. Exact mid-node of an 8-node quadrilateral

capable of producing finite element grids for design problems as well as extracting detailed blade information from Compressor Aerofoil Data-bases (CAD) containing three-dimensional aerofoil geometries.

Given the geometry of the gaspath the program starts by splining the hub and shroud by 'local' splines; in general 15 to 20 points per wall are supplied. The program then determines appropriate inlet and exit curves from the calculated wall curvatures. This defines the solution domain A–B–C–D of Figure 1. Since three-dimensional blade co-ordinates are usually defined independent of the gaspath, the blades are positioned by calculating the intersection of the given blade sectional information with the splined wall geometry. In our formulation we account for the exact geometry of the leading and trailing edges. The program furthermore produces all the necessary blade angle information required in the analysis. Since blade metal angles in the meridional direction change during each iteration we spline the three-dimensional camber line versus radius and axial position via the formulation defined in the Appendix. Once all blade rows' leading and trailing edges have

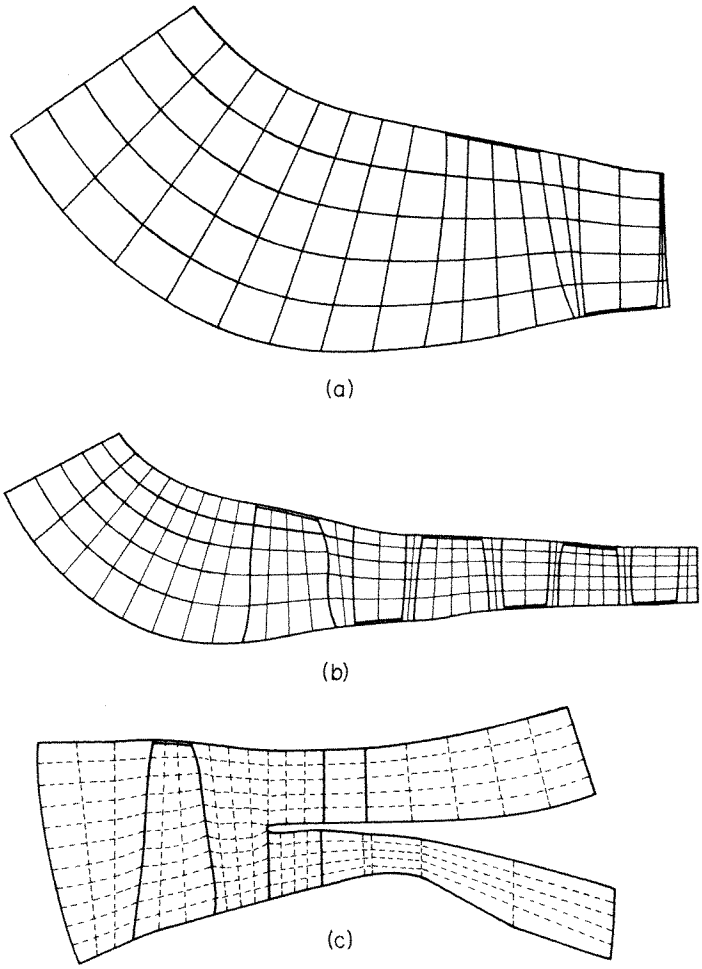

Figure 5. Typical grids used for test cases

been completely defined the program then isoparametrically divides the wall length within and between blade rows. These subdivisions are user selectable and have the capability of being distributed in an expanding/contracting fashion. Divisions in the radial direction are also interactively made in the same way. Typical grids are shown in Figures 5(a), (b). The mesh generation is also generalized to accept the possibility of a flow dividing splitter as in turbofans as shown in Figure 5(c).

4. SOLUTION PROCEDURE

(a) *Starting solution*

Since equation (7) is non-linear, the matrix $[K]$ is a function of the solution and the system is to be solved in an iterative fashion. In the present work the matrix $[K]$ and right hand side $\{F\}$ are re-formed at each iterative step with the terms in k_{ij} integrated via a (3×3) Gaussian integration scheme. The matrix is stored in a skyline form,[18] thereby reducing storage considerably, and is solved using an LL^{T} decomposition scheme. Since many of the nodes (hub and shroud) have Dirichlet boundary conditions, the matrix $[K]$ is reshuffled to eliminate these nodes from the solution. This again contributes greatly to the reduction of solution times. Because the matrix in (7) is symmetric and positive definite, it can be shown that under a transformation of the form

$$\{\Psi^*\}=[T]\{\Psi\} \tag{13}$$

where Ψ^* is a reduced vector of unknowns, one obtains

$$[K]^*\{\Psi^*\}=\{F\}^* \tag{14}$$

where $[K]^*=[T]^{\mathrm{T}}[K][T]$ and is also symmetric. Our initial guess for the solution is provided by solving (14) with $\{F\}^*$ set to zero.

It is found necessary to use an underrelaxation factor to damp the strong changes occurring in the first few iterations, which are usually divergent. Our factors, however, are not as low as those found in Reference 10. Moreover, as soon as the solution starts converging one can use an overrelaxation factor to speed up convergence. Figure 6 shows the convergence history of the analysis problem of the first stage of Figure 5(a). The results demonstrate that an underrelaxation factor of approximately 0·8 produces a steady, very rapid convergence. Multistaging changes this situation only slightly.

(b) *Solution update*

Once a reasonable first estimate of Ψ has been made for the entire field, one proceeds to calculate all thermodynamic variables at each station.

This begins by calculating the flow velocities from equations (2) and (3). These velocities are calculated using the nodal density values of the previous iteration. The calculation proceeds by applying conservation laws along streamlines between adjacent stations, these are:

In a duct:	Angular momentum,	$rC_u=\text{constant}$	(15)
In a stator:	Total enthalpy,	$H_0=\text{constant}$	(16)
In a rotor:	Rothalpy,	$I=\text{constant}$	(17)

To apply these conservation laws between adjacent stations, the streamline origin at each node of the station needs to be traced back. From Figure 3, the origin 0 of Ψ_4, on the edge

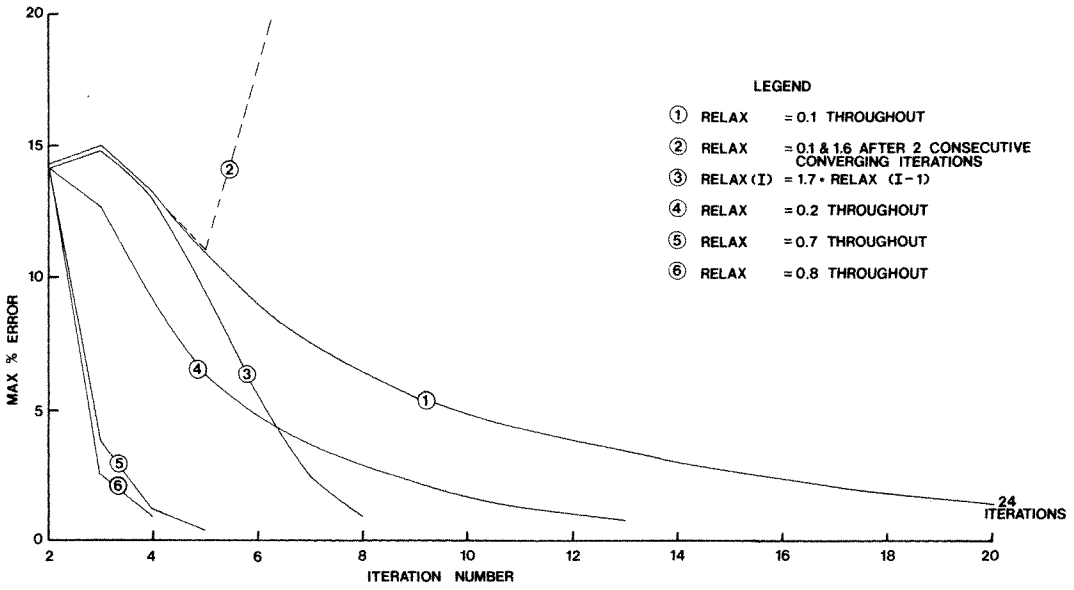

Figure 6. Convergence improvement with relaxation changes

(8–7–1), i.e. $\xi = -1$, is

$$\eta_0 = \frac{-(\Psi_7 - \Psi_1) + \sqrt{[(\Psi_7 - \Psi_1)^2 - 4(2\Psi_8 - 2\Psi_4)(\Psi_1 + \Psi_7 - 2\Psi_8)]}}{2(\Psi_1 + \Psi_7 - 2\Psi_8)} \tag{18}$$

This direct formula prevents the disadvantage of having to obtain the streamline origin by iteration.

Once the conservation property in question has been determined at nodes 2, 3, 4, 5 and 6 of each element, the loss model, if any, is applied. All thermodynamic properties are then calculated at these points with the reduced stagnation properties, using thermodynamic tables.[19]

(c) *Design mode*

Often the gas turbine designer is faced with the task of determining the optimum 3D blade shape to achieve a given pressure ratio with a given efficiency. Simple modifications to a through-flow analysis program can convert it to a design mode. In the present work several design modes have been implemented but only the two main ones are reported here.

In the first design mode one specifies the desired temperature rise across each stage along with estimated losses, say in the form $Z = \Delta P / \frac{1}{2}\rho_1 V_1^2$ at each nodal point of all trailing edges. Experience then dictates how such losses distribute themselves at other nodal points within the blade row. Furthermore the designer specifies flow angles at all stator nodes.

The second option is a quasi 3D design mode where angular momentum (rC_u) and recovery (defined in Figure 11) are specified at all rotor stations. As in the first design mode meridional flow angles and losses are specified at all stator nodes and can again be distributed non-linearly.

In the quasi-3D algorithm the above input serves as a starting point for an initial through-flow analysis. Such analysis then determines, inlet Mach number, inlet and exit flow

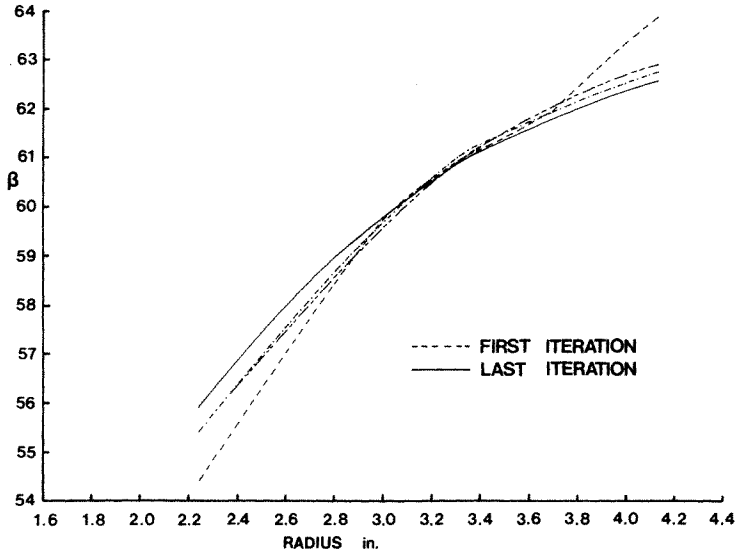

Figure 7. Convergence of β_{LE} with quasi 3D iterations

angles, and a distribution of intrablade streamtube heights. This information is then used to typically analyse from 5 to 10 blade-to-blade sections in each blade row.

The results of these blade-to-blade solutions are interpreted to yield new input to the through-flow code. Convergence, i.e. agreement between successive codes, is automatic. Figure 7 shows the convergence of one of the monitored parameters with iteration.

5. TEST CASES AND RESULTS

The FEM program has been thoroughly tested against the SCM and showed impressive gains in solution time. Both methods worked well in most tests but the SCM failed each time a gaspath with large curvatures was used or when too many intrablade stations were required. Streamlines for two axial compressors and a turbofan are shown in Figure 8.

Test Case 1: *theoretical annular diffuser*

An analytical solution[20] is available for the inlet and exit sections of the swirling flow in an annular diffuser. Since our program does not specify Ψ at inlet and exit, we have specified

$$\frac{1}{\rho}\frac{\mathrm{d}p}{\mathrm{d}r} = \frac{C_u^2}{r} = \Omega^2 r \tag{19}$$

so that

$$H_0 = \tfrac{1}{2}[C_x^2 + C_u^2] + \int \Omega^2 r \, \mathrm{d}r$$

At inlet

$$H_{0_i} = \tfrac{1}{2}[V^2 + (\Omega r)^2] + C_p T_\infty \quad \text{for forced vortex flow} \tag{20}$$

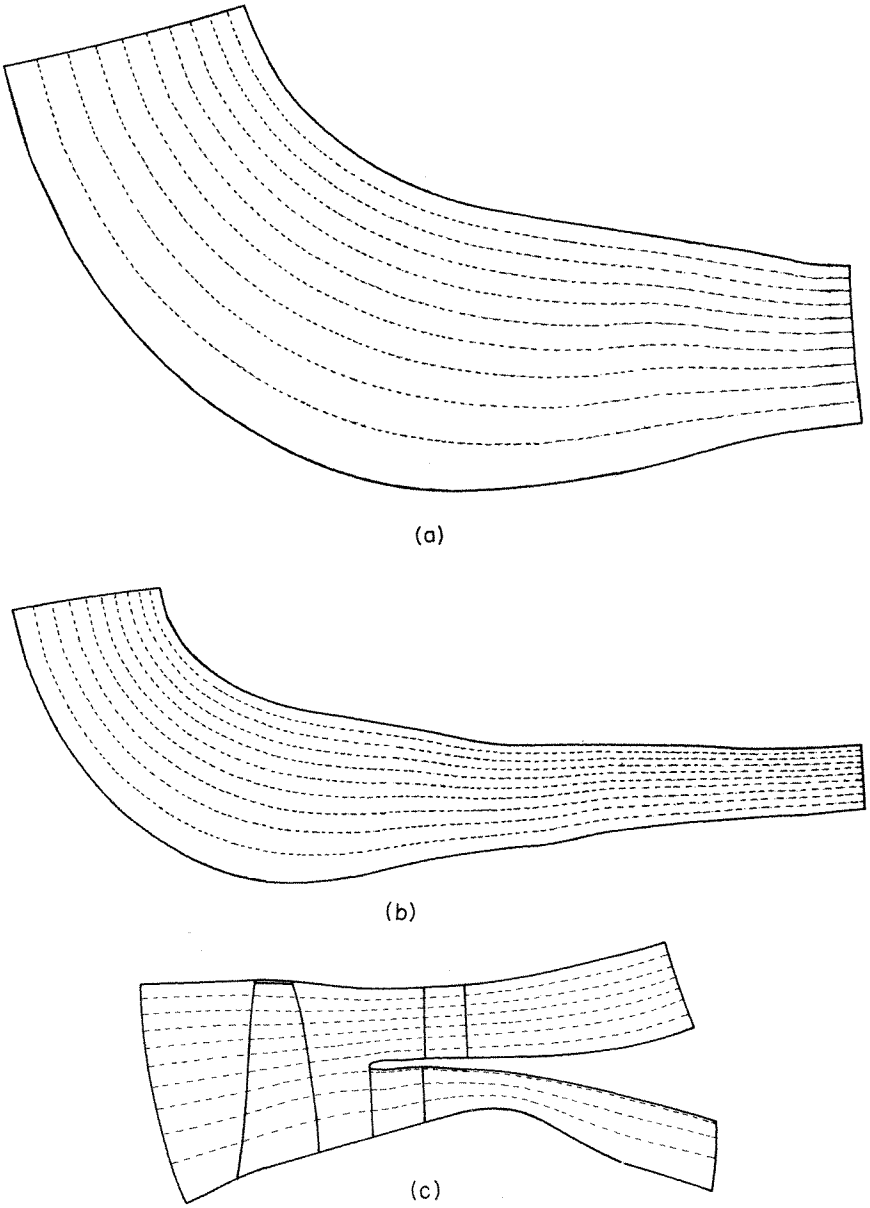

Figure 8. Streamline pattern for grids of Figure 5

and

$$T_{0_i} = H_{0_i}/C_p \tag{21}$$

$$P_{0_i} = P_{0_{hub}}(T_0/T_{0_{hub}})^{\gamma/(\gamma-1)} \tag{22}$$

$$P_{0_{hub}} = 14{\cdot}732, \text{ arbitrarily} \tag{23}$$

The geometry of the diffuser is given in Table I.

Table I

x	y	x	y
−23·0	2·0	−23·0	5·0
−21·5	2·0	−21·5	5·0
−20·0	2·0	−20·0	5·0
−18·5	2·0	−18·5	5·0
−17·0	2·05	−17·3	5·01
−15·5	2·3	−16·0	5·2
−14·0	2·9	−15·0	5·45
−12·5	3·8	−13·5	6·17
−10·8	5·0	−12·0	7·1
−9·3	5·95	−10·5	8·18
−8·2	6·5	−9·0	9·07
−7·0	6·8	−7·5	9·7
−5·8	7·0	−6·0	9·95
−4·5	7·0	−4·5	10·0
−3·0	7·0	−3·0	10·0
−1·5	7·0	−1·5	10·0
0·0	7·0	0·0	10·0

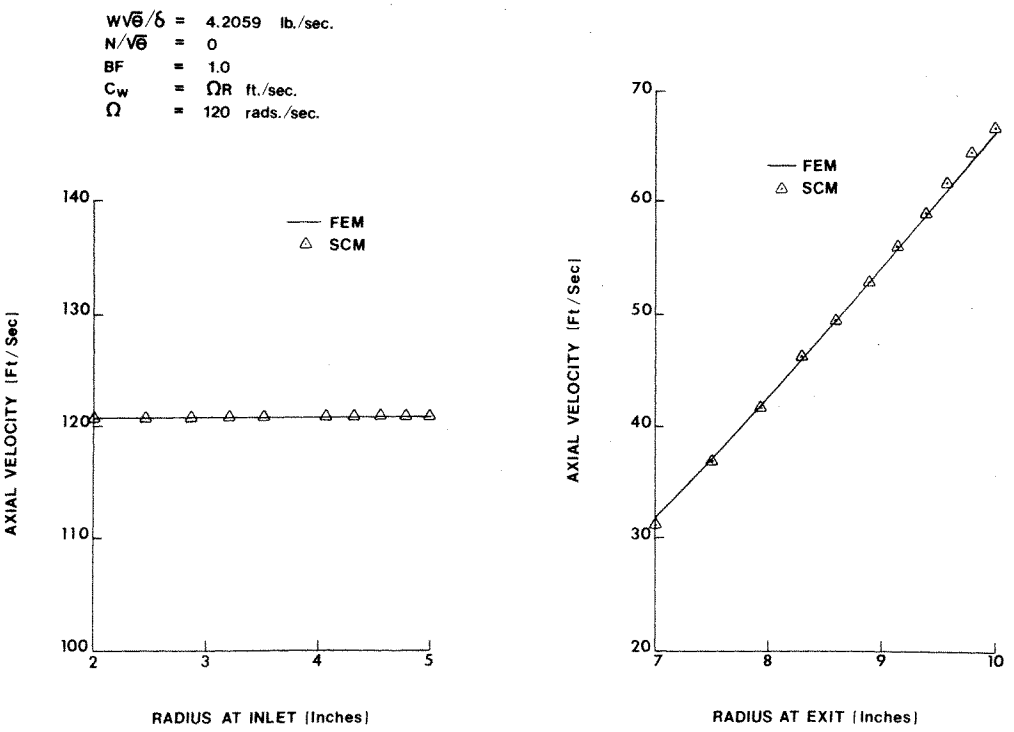

Figure 9. Theoretical annular diffuser, axial velocity

Convergence of the solution occurs in 4 iterations and solution times are about 4 seconds for 18 stations of 11 nodes each. The agreement with theory is excellent, at inlet and exit, as shown in Figures 9 and 10. Accurate solutions are obtainable with very few points at each station.

Test case 2: *free vortex compressor*

To further verify the correctness of the code we solve for the flow shown in Figure 11. It is a free-vortex flow in an axial compressor stage with radial blades. Losses are supplied in the form of the recovery shown in the same Figure. Again the results are comparable between FEM and SCM as demonstrated in Figure 12.

Solution times and convergence history are substantially different, however. The SCM program converges in 77 iterations with a corresponding execution time of 26 seconds, while the FEM converges in 4 iterations and uses 6 seconds of execution time.

Test case 3: *design of first stage of an axial compressor*

The method is tested in the through-flow design of a typical compressor. Figure 5(a) shows the FEM grid used in the first stage of this (4A+1C). Figure 8(a) shows the resulting streamline distribution for this case.

The design uses rC_u, recovery and blockage inputted at all stations. Some of these distributions are shown in Figure 13.

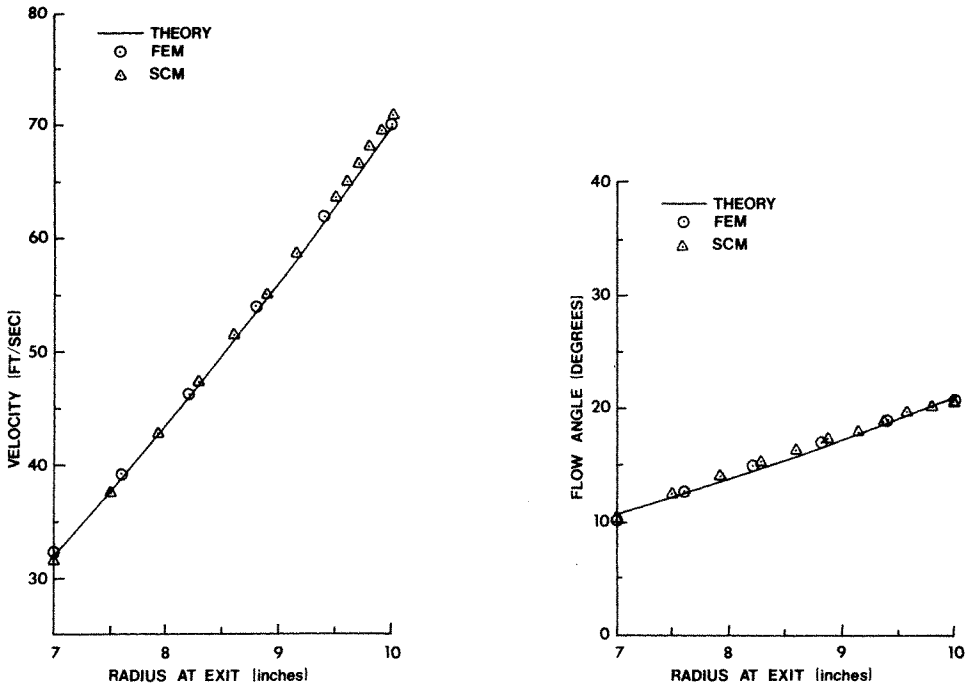

Figure 10. Theoretical annular diffuser, exit velocity and flow angle

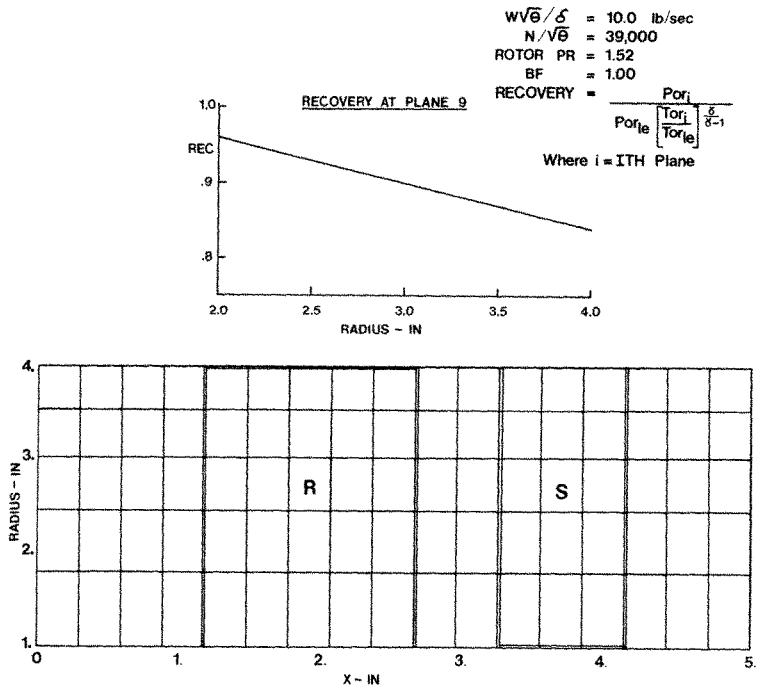

Figure 11. Cylindrical duct/free-vortex compressor

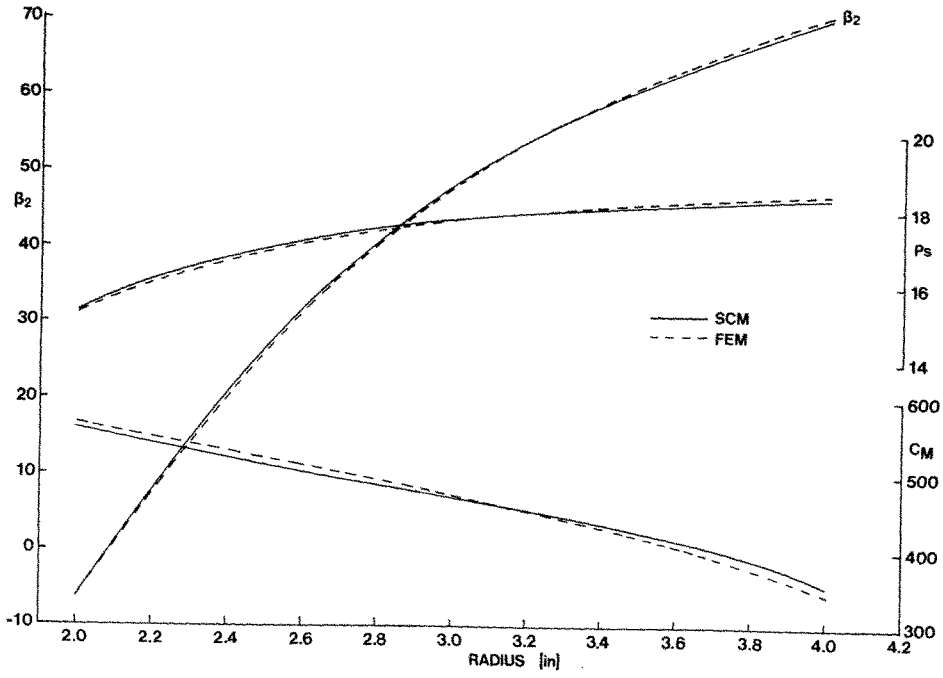

Figure 12. FEM vs. SCM for free-vortex compressor

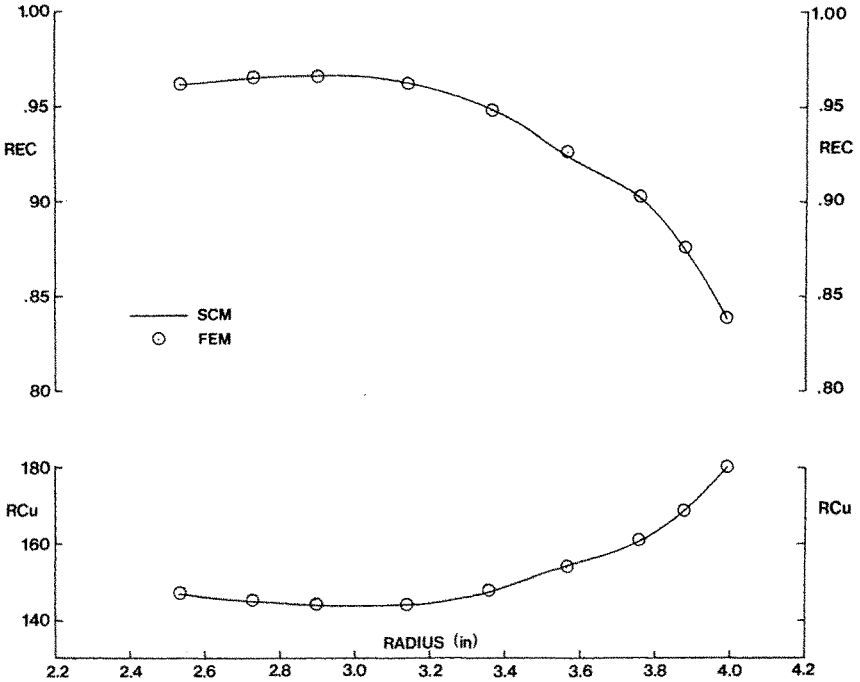

Figure 13. Supplied rC_u and recovery for compressor of Figure 5(a)

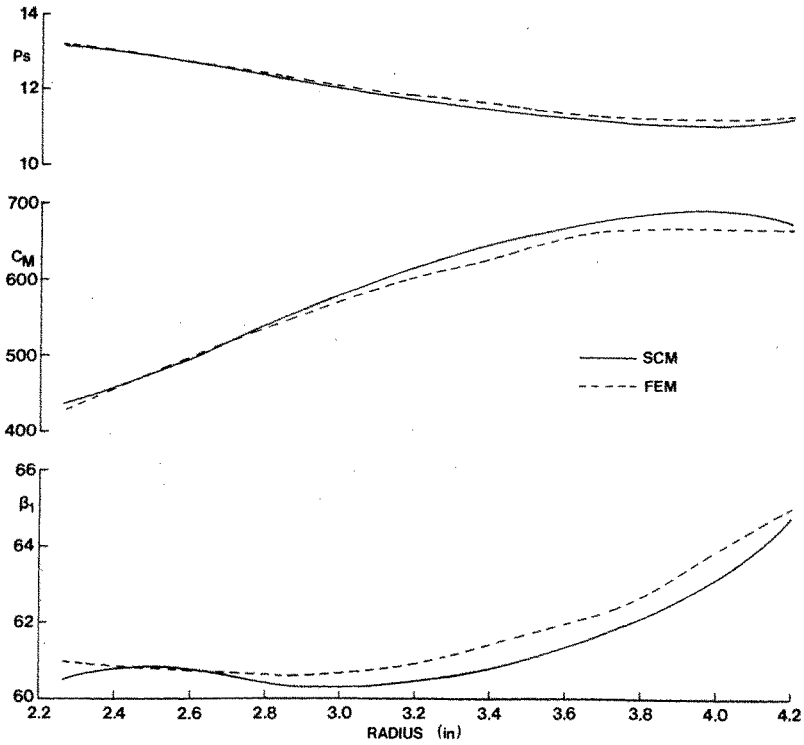

Figure 14. FEM vs. SCM results at rotor leading edge

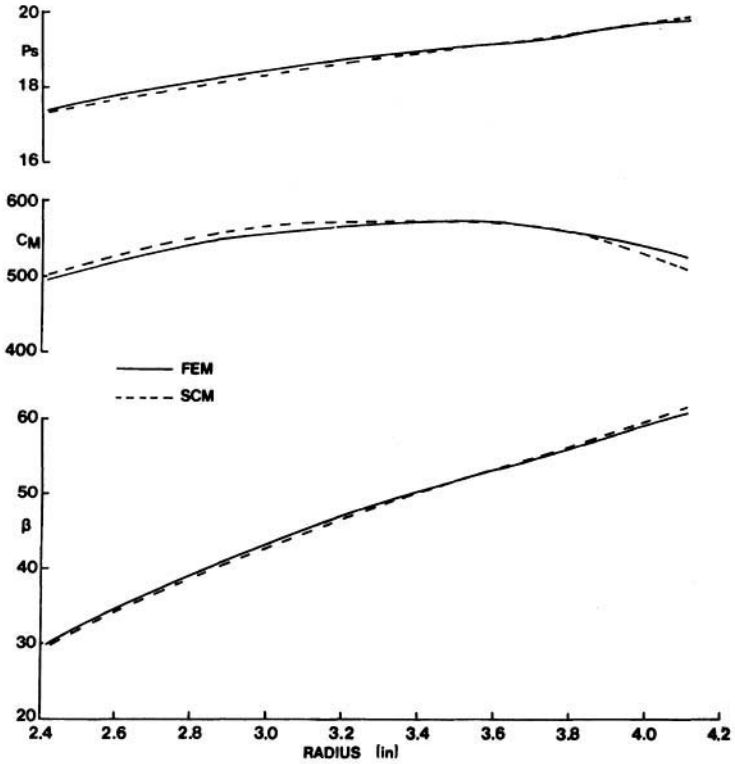

Figure 15. FEM vs. SCM results at second intrablade station

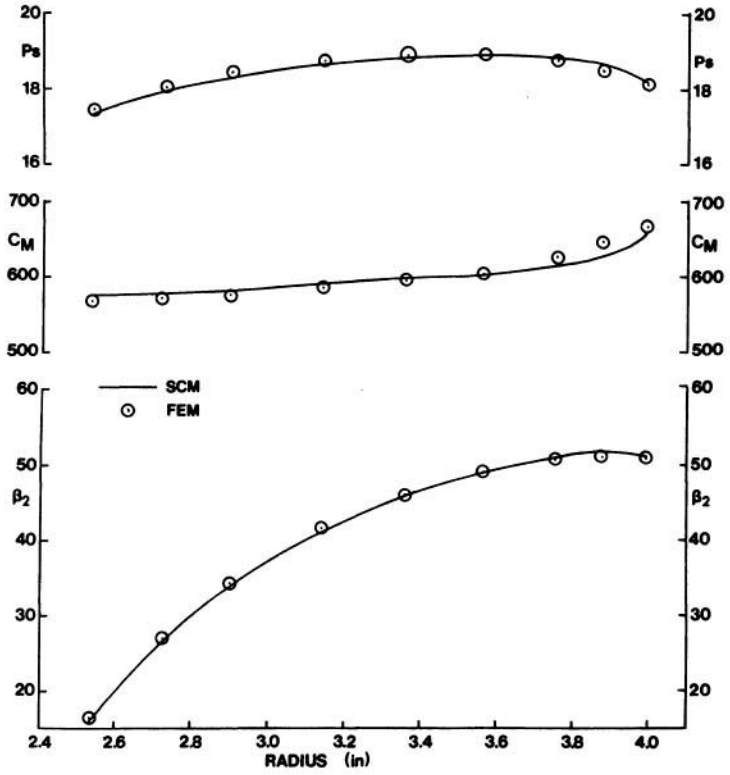

Figure 16. FEM vs. SCM results at rotor trailing edge

Typical FEM results plotted with SCM results are shown in Figures 14–16. Solution time comparisons are in the order of 2·5 : 1 in favour of finite elements. Three inside planes were used in the rotor with both methods.

Test case 4: *design of a typical axial compressor*

Figure 8(b) shows the streamlines generated for an axial stage of Figure 5(b). Selected results for the first stage of this design are shown in Figure 17.

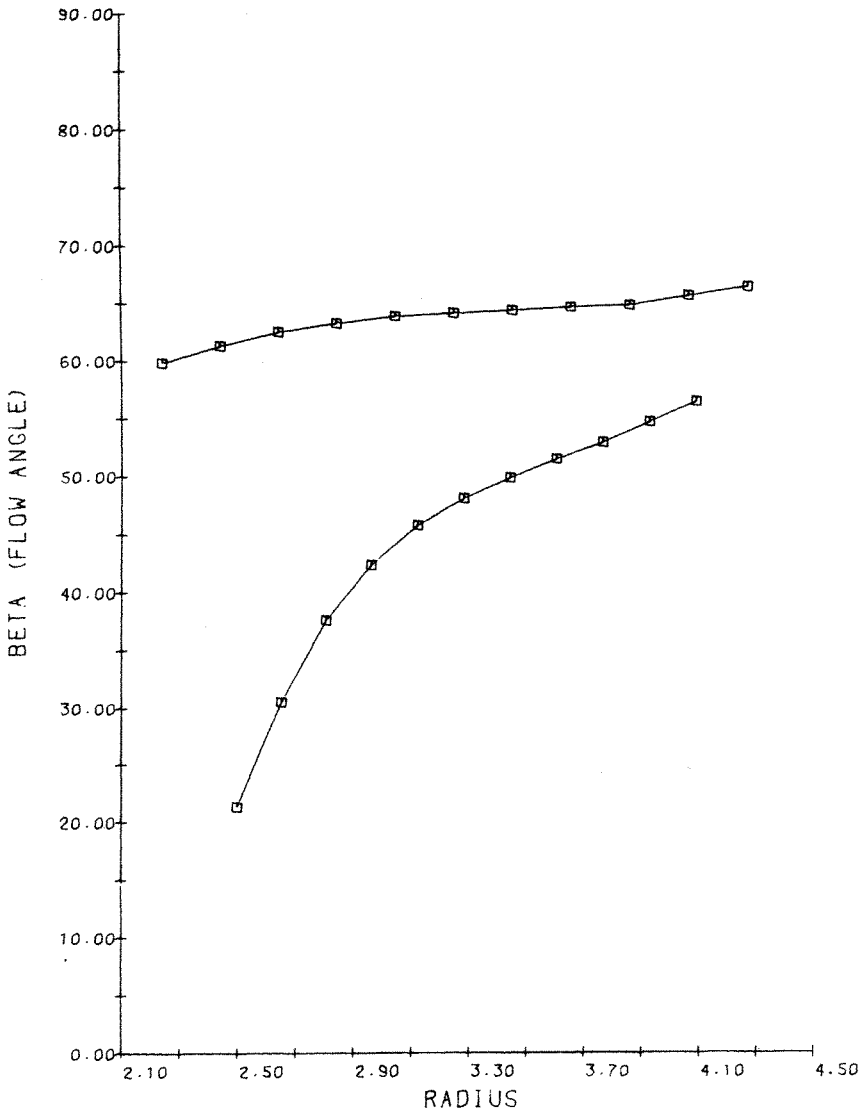

Figure 17. FEM results for first stage of Figure 5(b)

No comparison is made to SCM as all attemps to run SCM with 3 inside planes failed to converge.

CONCLUSIONS

A practical finite element through-flow approach has been demonstrated. Some industrially necessary practical aspects have been added and their effect shown. Direct comparisons to streamline curvature methods have been made for theoretical simple geometries as well as complex industrial geometries. The finite element method is shown to be at least from 2 to 4 times faster with no problems occurring under any geometries or curvatures. Applications to turbofans have been made and integration into a quasi-3D package has been demonstrated.

ACKNOWLEDGMENTS

The authors would like to thank D. Tsang and A. Hammerschmidt for programming the mesh generation package and E. Dueck and A. Mawatari for the metal angle definition formulation. This work was partially supported under PRAI grant P-7901 and grant A-3662 of the Natural Sciences and Engineering Council of Canada (NSERC).

APPENDIX. METAL ANGLE DEFINITION ALONG ARBITRARY STREAM SURFACES

Definition of the blade angle

Given the 3D camber line the blade angles are defined as follows:

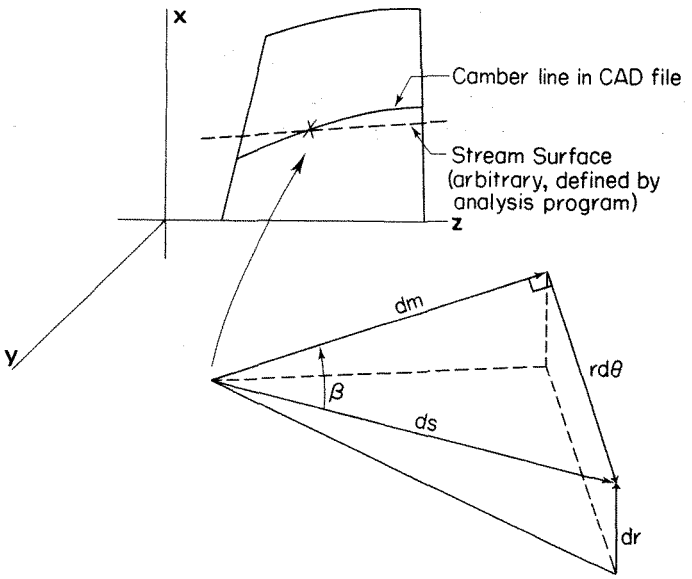

Figure 18

$$\beta = \cos^{-1}\left(\frac{dm}{ds}\right) \tag{24}$$

or

$$\tan\beta = r\frac{\partial\theta}{\partial m} \tag{25}$$

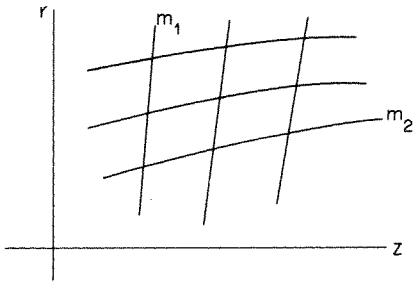

Figure 19

Definition of the mesh orientation

The finite element mesh is defined in the meridional plane, which is in the z–r system.

Each mesh line, in a blade row, is fitted with a cubic spline through the mesh points. This is done for each of the m_1 and m_2 mesh lines shown in Figure 19. This is especially important at the leading and trailing edges as they are curved.

Therefore,

$$r_{m1} = F(z_{m1}) \tag{26}$$

and

$$z_{m2} = G(r_{m2})$$

From the above splines we may obtain dr/dz.

Calculation of the blade angle along the specific mesh lines

A surface of revolution is obtained by rotating the mesh line about the axis of the engine (z). We can obtain, by splining, a camber line that is the intersection of the surface of revolution and the blade.

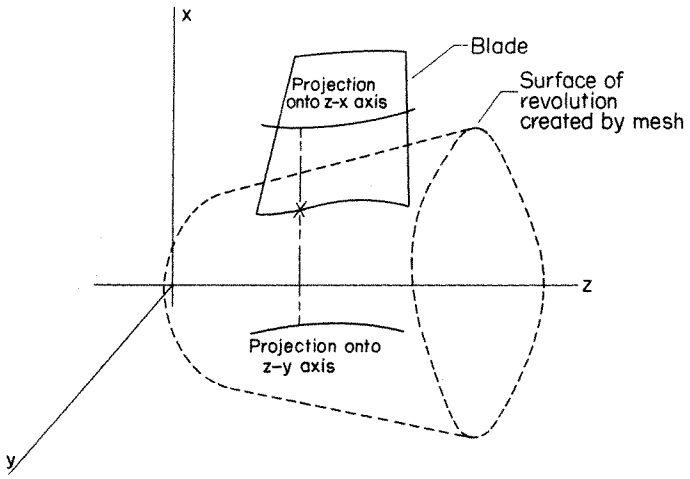

Figure 20

The 3D camber line can then be defined by two 2D splines, one being in the (z, x) plane and the other being in the (z, y) plane.

$$\begin{aligned} z\text{–}x \text{ plane} \quad & x = f_1(z) \\ y\text{–}z \text{ plane} \quad & y = f_2(z) \end{aligned} \tag{27}$$

From equation (24)

$$\cos\beta = \frac{dm}{ds} = \frac{\sqrt{[(dr)^2+(dz)^2]}}{\sqrt{[(dx)^2+(dy)^2+(dz)^2]}} = \frac{\sqrt{\left[\left(\frac{dr}{dz}\right)^2+1\right]}}{\sqrt{\left[\left(\frac{dx}{dz}\right)^2+\left(\frac{dy}{dz}\right)^2+1\right]}} \tag{28}$$

Differentiating (26) and (27) so that

$$\frac{dr}{dz} = F'(z); \qquad \frac{dx}{dz} = f_1'(z); \qquad \frac{dy}{dz} = f_2'(z)$$

and substituting the above derivatives into equation (28) we can calculate the β along the mesh line as being

$$\cos\beta = \frac{\sqrt{[(F')^2+1]}}{\sqrt{[(f_1')^2+(f_2')^2+1]}} \tag{29}$$

Calculation of the blade angle along a given meridional direction at a mesh point

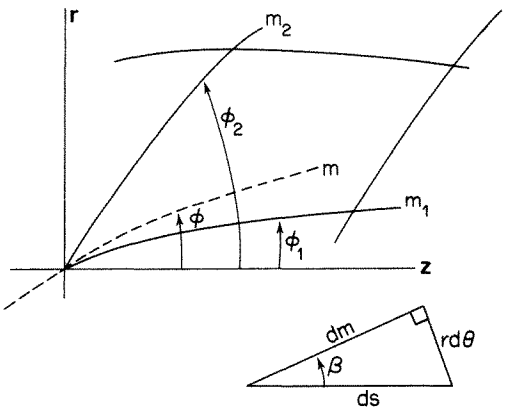

Figure 21

At a given mesh point in the local meridional plane one uses equation (25) in the cylindrical system instead of equation (24).

$$\tan\beta = r\frac{\partial\theta}{\partial m} \tag{30}$$

By taking directional derivatives of θ along the direction of m in the (z, r) plane one gets

$$\frac{\partial\theta}{\partial m}=\cos\phi\frac{\partial\theta}{\partial z}+\sin\phi\frac{\partial\theta}{\partial r} \tag{31}$$

applying this relation along mesh lines m_1 and m_2

$$\frac{\partial\theta}{\partial m_1}=\cos\phi_1\frac{\partial\theta}{\partial z}+\sin\phi_1\frac{\partial\theta}{\partial r} \tag{32}$$

$$\frac{\partial\theta}{\partial m_2}=\cos\phi_2\frac{\partial\theta}{\partial z}+\sin\phi_2\frac{\partial\theta}{\partial r} \tag{33}$$

From (32) and (33)

$$\frac{\partial\theta}{\partial z}=\frac{1}{\sin(\phi_2-\phi_1)}\left(\sin\phi_2\frac{\partial\theta}{\partial m_1}-\sin\phi_1\frac{\partial\theta}{\partial m_2}\right) \tag{34}$$

$$\frac{\partial\theta}{\partial r}=\frac{1}{\sin(\phi_2-\phi_1)}\left(-\cos\phi_2\frac{\partial\theta}{\partial m_1}+\cos\phi_1\frac{\partial\theta}{\partial m_2}\right) \tag{35}$$

From equation (30)

$$\frac{\partial\theta}{\partial m}=\frac{1}{r}\tan\beta \tag{36}$$

Therefore the blade metal angles along the mesh lines m_1 and m_2 become β_1 and β_2 so that

$$\begin{aligned}\frac{\partial\theta}{\partial m_1}&=\frac{1}{r}\tan\beta_1\\ \frac{\partial\theta}{\partial m_2}&=\frac{1}{r}\tan\beta_2\end{aligned} \tag{37}$$

Substituting equations (34)–(37) into equation (31) one obtains

$$\tan\beta=\frac{1}{\sin(\phi_2-\phi_1)}(\sin(\phi_2-\phi)\tan\beta_1+\sin(\phi-\phi_1)\tan\beta_2) \tag{36}$$

thus storing β_1, β_2, ϕ_1 and ϕ_2 in the mesh generation stage one can determine β for any arbitrary stream surface inclined at angle ϕ.

REFERENCES

1. C. H. Wu, 'A general theory of three dimensional flow in subsonic, and supersonic turbomachines of axial, radial and mixed flow type', *NACA TN 2604* (1952).
2. R. A. Novak, 'Streamline curvature computing procedures for fluid flow problems', *J. Engg. for Power, Trans. ASME*, **89,** 478–490 (1967).
3. R. A. Novak and R. M. Hearsey, 'A nearly three-dimensional intrablade computing system for turbomachinery', *J. Fluids Engg., Trans. ASME*, **99** (1), 154–166 (1977).
4. D. H. Frost, 'A streamline curvature through-flow computer program for analysing the flow through axial flow turbomachines', *N.G.T.E. Report No. R.312* (1970).
5. H. Marsh, 'A digital computer program for the through-flow fluid mechanics in an arbirtary turbomachine using a matrix method', *ARC R & M 3509* (1966).
6. T. Katsanis, 'Use of arbitrary quasi-orthogonals for calculating flow distribution in the meridional plane of a turbomachine', *NASA-TN-D-2546* (1964).
7. D. J. Denton, 'Throughflow calculations for transonic axial flow turbines', *J. Engg. for Power, Trans. ASME*, **100,** (2), 212–218 (1978).

8. W. R. Davis and D. A. J. Millar, 'A discussion of the Marsh matrix technique applied to fluid flow problems', *Canadian Aeronautics and Space Journal*, **5** (2), 64–70 (1972).
9. W. R. Davis and D. A. J. Millar, 'A comparison of the matrix and streamline curvature methods of axial flow turbomachinery analysis, from a user's point of view', *J. Engg. for Power, Trans. ASME* **97** (4), 549–560.
10. Ch. Hirsch and G. Warzee, 'A finite element method for through-flow calculations in turbomachines', *J. Fluids Engg., Trans. ASME*, **98,** 403–421 (1976).
11. D. Adler and Y. Krimerman, 'The numerical calculation of the meridional flow field in turbomachines using the finite element method', *Israel J. Tech*, **12** (1974).
12. G. C. Oates, C. J. Knight and G. F. Carey, 'A variational formulation of the compressible throughflow problem', *J. Engg. Power*, **98,** 1–8 (1979).
13. W. G. Habashi, 'Numerical methods of turbomachinery', Chapter 8 in *Recent Advances in Numerical Methods in Fluids*, (C. Taylor and K. Morgan, (eds.)) Pineridge Press, 1980.
14. P. W. McDonald, 'The computation of transonic flow through two-dimensional gas turbine cascades', *ASME paper 71-GT-89* (1971).
15. W. G. Habashi and P. L. Kotiuga, 'Numerical solution of transonic cascade flows', *Paper presented at the ASME Century 2 Emerging Technology Conferences*, Aerospace Conference, San Francisco (1980).
16. W. G. Habashi and M. M. Hafez, 'Finite element stream function solutions for transonic turbomachinery flows', *AIAA Paper 82–1268, AIAA/SAE/ASME 18th Joint Propulsion Conference*, Cleveland, June (1982).
17. H. Deconinck and C. H. Hirsch, 'Finite element methods for transonic blade-to-blade calculations in turbomachines', *ASME paper 81-GT-5, ASME International Gas Turbine Conference*, Houston, Texas (1981).
18. K. J. Bathe and E. L. Wilson, *Numerical Methods in Finite Element Analysis*, Prentice Hall, 1976.
19. M. S. Chappell and E. P. Cockshutt, 'Gas turbine cycle calculations: thermodynaic data tables for air and combustion products for three systems of units', *NRC Aeronautical Report LR-579* (1974).
20. G. K. Batchelor, *An Introduction to Fluid Dynamics*, Cambridge University press, 1970, pp. 543–558.